

PHYSICAL CHEMISTRY OF NANOCCLUSERS
AND NANOMATERIALS

Enhanced Photocatalytic and Photoluminescence Properties of Ce and Dy Co-Doped ZnO Nanoparticles

Syed Irtiq^a and Atikur Rahman^{a,*}

^aDepartment of Metallurgical and Materials Engineering, National Institute of Technology Srinagar, Hazratbal, Srinagar, 190006 India

*e-mail: atikurrhmn@gmail.com, atikurrhmn@nitsri.net

Received June 25, 2020; revised June 25, 2020; accepted October 5, 2020

Abstract—Cerium and dysprosium co-doped ZnO nanoparticles were synthesized through a simple co-precipitation approach at low temperature. X-ray diffraction was used for the structure and purity analysis of the samples prepared. A hexagonal wurtzite structure was observed with no secondary peaks. The average particle size was ~35 nm. Morphology was studied using scanning electron microscopy. A change in morphology from elongated nanorods to nanoflowers was observed as the concentration of dopants increased. Photoluminescence spectra confirmed the shift of absorption edge towards the visible region of the solar spectrum. Red shift was confirmed by UV–Vis spectroscopy which also revealed the narrowing of bandgap in co-doped samples. The photocatalytic activity of the nanoparticles was evaluated in photodegradation of rhodamine B (RhB) under UV irradiation. The experiment revealed a total degradation of the organic molecules indicated by the elimination of the dye color. The results showed that ZnO photocatalyst, co-doped with cerium and dysprosium (Zn_{0.90}Ce_{0.05}Dy_{0.05}O), exhibited much improved photocatalytic performance (98% degradation) in comparison to un-doped ZnO. The enhanced photocatalytic performance of co-doped samples could be explained by an increase in the amount of surface oxygen vacancies, improved absorption capacity and delayed recombination of photo generated electrons and holes owing to creation of trap states in the bandgap of ZnO.

Keywords: ZnO, Ce and Dy co-doping, co-precipitation, photoluminescence, photocatalyst, rhodamine B, rare earths

DOI: 10.1134/S0036024421090260

INTRODUCTION

In recent times, semiconductor nanomaterials have been vital in the advancement of electronics and technology. Some semiconductors such as TiO₂, ZnS, ZnO, ITO, CdSe, etc. exhibit excellent optical properties [1]. Amongst them, ZnO being the II–VI semiconductor has a high binding energy at room temperature. ZnO also has a wide bandgap (3.37 eV), high chemical stability and high melting point (1975°C). It is the most commonly used semiconductor in optoelectronic applications like photocatalysis, solar cells and field emission displays due to its low cost, easy synthesis, low toxicity, electron transport capability and low crystallization temperature [2–7].

Physical properties of semiconductor nanomaterials are tuned by intentional incorporation of impurity ions into the host lattice-doping [8–12]. Doping is seen to modulate the optoelectronic and magnetic properties of ZnO. Radiative transitions of 4f electrons of rare earth ions have been under research because of their unique luminescent and recombination sites for electron-hole pairs [13]. Semiconductor based photocatalysts such as ZnO are of pivotal importance in alleviating the global concerns primarily related to the

treatment of waste water. Water pollution and scarcity of water are the major scientific challenges impacting billions of people world over. Textile industry and dye production units produce enormous amount of effluent water containing intense colored toxic dyes. Rhodamine B (RhB) is the most widely used dye in the textile industry and dye production units owing to its high stability. However, it is extremely harmful to human and aquatic life due to its carcinogenic and mutagenic nature. Hence degradation and decomposition of Rhodamine B dye is absolutely important for conservation of water, aquatic life and human safety [14]. Photocatalysis has emerged as the most efficient, low cost and green process for waste water treatment. Many semiconductor nanomaterials like TiO₂, SnO₂, ZnO have been of high interest for researchers due to their excellent photocatalytic performance. Among the semiconductive oxides, ZnO is most suitable for photocatalysis and degradation of organic compounds because of its non-toxicity, chemical and corrosion, stability and low cost [15–19]. However the major shortcomings of un-doped ZnO nanoparticles for practical applications pertain to its narrow spectral range of response ($\lambda < 380$ nm) which comprises only

6–8% of solar energy while as visible light contributes to 46% of the spectrum. Thus, to obtain a better photocatalyst from ZnO, its absorption edge needs to be moved from UV to visible region. Further, less separation gap between electrons and holes, generated after a high energy photon absorption by ZnO, leads to recombination and energy dissipation within nanoseconds. As photogenerated electrons and holes can act as powerful oxidizing and reducing agents respectively, a better charge separation between them can pave the way for redox reactions, and, as a result, improved photocatalysis can be achieved [20, 21]. These improvements in photocatalytic properties can be achieved through doping with rare earth ions [22–26]. Doping of lanthanides in ZnO have been studied with metals like cerium (Ce), lanthanum (La), and dysprosium (Dy) [27–31]. Among the rare earth dopants with 4f configuration, cerium is particularly interesting owing to its larger ionic size which causes a localized charge perturbation when substituted into the ZnO lattice, hence increasing its photocatalytic activity [32–36]. Doping of ZnO with rare earth ions is extensively studied, hardly leaving any scope for further investigations in this area. However, a combination of rare earth dopings can be investigated for various advantages over the single metal doping. Very few works are available on these combination doping studies [37–43]. Our curiosity towards investigating the impact of combination doping on optical properties of semiconductors, motivated us for a detailed analysis of Ce and Dy co-doping into ZnO matrix. To our excitement, improvements in the optical properties were observed on three fronts. We, herein, report an optimized and enhanced photocatalytic performance of ZnO nanoparticles with better optical bandgap dependant on the co-dopant concentrations, a prolonged separation between photogenerated charge carriers due to induced trap levels in the bandgap of ZnO and a red shift towards visible region for productive utilization of solar energy.

Rare earth ion doped ZnO nanoparticles have been synthesized by various methods like forced hydrolysis [44], pulsed laser deposition [45], and combustion method [46]. These methods are complex and usually require high temperatures, costly machinery and harmful chemicals.

A simple, cost effective and environmental friendly method of co-precipitation has been used for the synthesizing Ce and Dy co-doped ZnO nanoparticles in the present work. ZnO nanoparticles with an increasing concentration of co-dopants i.e., $\text{Zn}_{0.98}\text{Ce}_{0.01}\text{Dy}_{0.01}\text{O}$, $\text{Zn}_{0.96}\text{Ce}_{0.02}\text{Dy}_{0.02}\text{O}$, $\text{Zn}_{0.94}\text{Ce}_{0.03}\text{Dy}_{0.03}\text{O}$, $\text{Zn}_{0.92}\text{Ce}_{0.04}\text{Dy}_{0.04}\text{O}$ and $\text{Zn}_{0.90}\text{Ce}_{0.05}\text{Dy}_{0.05}\text{O}$ were synthesized for comparative optical studies. Structural, morphological, optical and photoluminescence features of the co-doped samples were studied using XRD, SEM, UV–Vis spectrophotometer and photoluminescence, respectively, in the

present work. The photocatalytic performance of the pure and co-doped samples was studied by observing the degradation of rhodamine B dye under UV light irradiation. The degradation of harmful organic waste and consequent removal of color was considerably improved with Ce and Dy co-doped ZnO nanoparticles as photocatalyst, in comparison to the un-doped ZnO nanoparticles. The mechanism of degradation of rhodamine B dye with nano photocatalyst is also discussed in current work.

EXPERIMENTAL

A facile, low cost and ecofriendly co-precipitation route was used for synthesizing Ce and Dy co-doped ZnO nanoparticles, i.e. ($\text{Zn}_{0.98}\text{Ce}_{0.01}\text{Dy}_{0.01}\text{O}$, $\text{Zn}_{0.96}\text{Ce}_{0.02}\text{Dy}_{0.02}\text{O}$, $\text{Zn}_{0.94}\text{Ce}_{0.03}\text{Dy}_{0.03}\text{O}$, $\text{Zn}_{0.92}\text{Ce}_{0.04}\text{Dy}_{0.04}\text{O}$, and $\text{Zn}_{0.90}\text{Ce}_{0.05}\text{Dy}_{0.05}\text{O}$). The mole fraction of dopant ions in the co-doped ZnO nanoparticles was maintained by adjusting the weight ratio of dopants, Ce and Dy, to host zinc. The starting salt and dopant sources used i.e., host (zinc(II) acetate dihydrate [$\text{Zn}(\text{COOCH}_3)_2 \cdot 2(\text{H}_2\text{O})$] and dopants cerium(III) acetate sesquihydrate [$\text{Ce}(\text{CH}_3\text{COO})_3 \cdot 1.5(\text{H}_2\text{O})$], dysprosium(III) acetate tetrahydrate [$\text{Dy}(\text{CH}_3\text{COO})_3 \cdot 4\text{H}_2\text{O}$] were of high purity (Sigma Aldrich, 99% purity). The reagents were used without further purification. Distilled water was used as solvent and diethylamine was used as a base and stabilizing agent. To begin with, pure ZnO nanoparticles were synthesized. For this 0.5 M zinc acetate solution was prepared in a beaker at 60°C and 5 mL of diethylamine was slowly added to it. The reaction was carried out for 30 min followed by heating at 180°C. The precipitate was centrifuged and annealed at 500°C in a muffle furnace for 1 h.

To prepare the Ce and Dy co-doped ZnO nanoparticles, the solutions of dopant ions (cerium(III) acetate sesquihydrate and dysprosium(III) acetate tetrahydrate) of mole fractions varying from 0.01–0.05 with concentration step of 0.01 were prepared in distilled water. These solutions were then added to the solution of 0.5 M zinc acetate. Afterwards, 5 mL of diethylamine was slowly dropwise added to the above solution under continuous stirring at 60°C. The solution was further heated and stirred for 1 h. The final product was centrifuged, washed with ethanol and annealed at 500°C in a muffle furnace. Table 1 presents the standard conditions and molarities used for the synthesis of Ce and Dy co-doped ZnO nanoparticles.

The structural features of nanoparticles were analyzed using X-ray diffractometer with CuK_α radiation ($k = 1.54052 \text{ \AA}$). The diffraction patterns were recorded in the range of 2θ from 10° to 90° with a step of 0.01°. The morphology of undoped ZnO and Ce and Dy co-doped ZnO nanoparticles was studied using SEM. Horiba LabRam spectroscopy system with an excitation source wavelength of 325 nm and an

accumulation time of 2 s was used to record the PL spectrum of the un-doped and co-doped ZnO nanoparticles. Optical absorbance was measured on UV–Vis spectrophotometer (Perkin Elmer, Lambda 35) in the wavelength range from 200–800 nm.

Photocatalytic Activity Measurement

To measure the photocatalytic activity of un-doped and Ce and Dy co-doped ZnO nanoparticles, a 10 ppm solution of rhodamine B dye was prepared. 10 mL of this solution was taken in 250 mL beaker, which was then diluted with distilled water to make a total of 40 mL solution. The prepared nanoparticles (40 mg) were added to the solution under constant stirring. The solution was wrapped, kept in dark and stirred for half an hour to disperse the nanoparticles (photocatalyst) and to establish the adsorption–desorption equilibrium. Afterwards, the solution was irradiated with UV light in the photocatalytic reactor (M/S Technistro, Nagpur, Maharashtra) fitted with high pressure mercury lamp with 450 W power (operating voltage 110–220 V), whilst the stirring was continued. An aliquot of 3 mL was withdrawn after every 10 min and immediately centrifuged to remove catalyst nanoparticles. The absorbance of the samples was measured with a UV–Vis spectrophotometer (Perkin Elmer Lambda 35) between 400–600 nm wavelength. The gradual decrease in the absorbance of dye, together with the removal of color, confirmed the degradation of rhodamine B dye with un-doped and Ce and Dy co-doped ZnO nanoparticles as photocatalyst.

RESULTS AND DISCUSSION

Structural Analysis

XRD pattern of un-doped and Ce and Dy co-doped ZnO nanoparticles are shown in Fig. 1a. The prepared materials displayed a hexagonal wurtzite structure and their diffraction patterns correspond to the International Centre for Diffraction Data (ICDD) database no. 01-070-8072. The peaks corresponding to reflections from (100), (002), (101), (102), (110), (103), (112), and (201) planes belonged to varied (*hkl*) families suggesting that all the samples had polycrystalline nature. No secondary peaks were observed except ZnO suggesting that all samples formed were pure phase. The dopant ions Ce³⁺ and Dy³⁺ have ionic radii of 1.03 and 0.91 Å, respectively, which is quite large when compared to the ionic radius of parent Zn²⁺ ion (0.72 Å). This leads to a slight distortion in the lattice of ZnO. Further, there was a shift towards higher angle in the doped nanoparticles as compared to un-doped nanoparticles as shown in Fig. 1b, which

Table 1. Standard conditions for synthesis of Ce, Dy co-doped ZnO nanoparticles (0.5 M zinc acetate, 5 mL of diethylamine, x_{Ce} and x_{Dy} are concentration of cerium acetate and dysprosium acetate, respectively)

x_{Ce} , M	x_{Dy} , M
0.000	0.000
0.005	0.005
0.010	0.010
0.015	0.015
0.020	0.020
0.025	0.025

confirms substitutional doping of Ce and Dy ions into the ZnO matrix.

The formulas below were used for the calculation of crystallite size and lattice constants and the values of same are stated in Table 2

$$a = \frac{\lambda}{\sqrt[3]{\sin \theta}}, \quad (1)$$

$$b = \frac{\lambda}{\sin \theta}, \quad (2)$$

$$D = \frac{K\lambda}{\beta \cos \theta}, \quad (3)$$

where λ is the wavelength of X-ray radiation, i.e., 1.5406 Å, θ is the diffraction angle, K is the shape factor, D is the crystallite size, while β is the full width half maximum of a diffraction peak. It can be seen from Table 1, the crystallite size decreases with increase in doping concentration. Un-doped nanoparticles have a crystallite size of 47 nm, while Zn_{0.90}Ce_{0.05}Dy_{0.05}O showed a crystallite size of 30 nm. Mismatch of ionic radii of parent and dopant ions causes an increase in bond length which gets reflected in increased values of lattice constants a and c as shown in Table 2.

Morphological Studies

The SEM micrographs of un-doped ZnO and Ce and Dy co-doped ZnO nanoparticles are displayed in Figs. 2a–2e. SEM images confirm the XRD results. The particle size decreases as the concentration of co-dopants increases. The mismatch of ionic radii between parent Zn²⁺ ion (0.72 Å) and dopant Ce³⁺ (1.03 Å) and Dy³⁺ (0.91 Å) ions leads to lattice strain which eventually leads to smaller grain size of the co-doped nanoparticles. Also the co-doped ZnO nanoparticles exhibit flower like morphology, this can be possibly due to the doping with Ce³⁺ ions which play a pivotal role in capping of co-doped nanoparticles formed during nucleation [47]. Ce³⁺ ions in presence of strongly absorbed stabilizing agent diethylamine cause

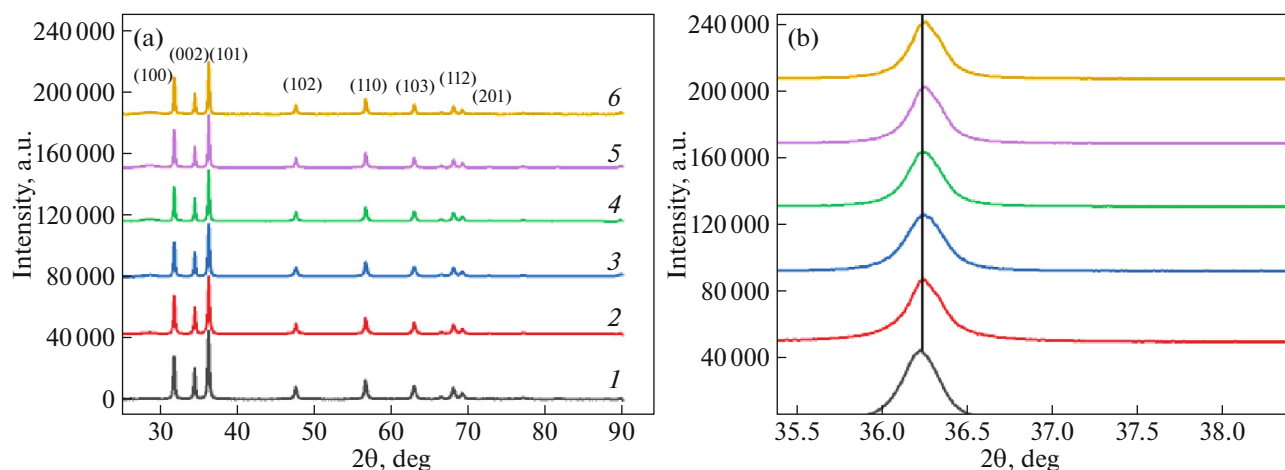


Fig. 1. (a) XRD patterns of un-doped ZnO (1) and Ce,Dy co-doped ZnO nanoparticles (2— $\text{Zn}_{0.98}\text{Ce}_{0.01}\text{Dy}_{0.01}\text{O}$, 3— $\text{Zn}_{0.96}\text{Ce}_{0.02}\text{Dy}_{0.02}\text{O}$, 4— $\text{Zn}_{0.94}\text{Ce}_{0.03}\text{Dy}_{0.03}\text{O}$, 5— $\text{Zn}_{0.92}\text{Ce}_{0.04}\text{Dy}_{0.04}\text{O}$, and 6— $\text{Zn}_{0.90}\text{Ce}_{0.05}\text{Dy}_{0.05}\text{O}$); (b) expanded XRD pattern showing peak shift towards higher angle values with increase in co-dopant concentration.

steric hindrances which lead to formation of flowers like structure of Ce and Dy co-doped ZnO nanoparticles. This phenomenon can be further elaborated on the basis of growth and nucleation of nanoparticles. The formation of seed nuclei is initiated by the precursor, which grow into long rods by Ostwald ripening effect where larger particles enlarge at the expense of smaller particles. This mechanism is facilitated by a solvent and the various subunits formed by this method are connected by orientation attachment process leading to flower like structure [48].

Optical Studies

The study of optical properties plays an important role in selection of nanomaterials for various applications. To investigate the optical properties like bandgap, additional energy levels and absorption edge of pure and Ce and Dy co-doped ZnO nanoparticles, we used UV-Vis spectrometry in the wavelength range 200–800 nm. The absorbance spectra of un-doped

ZnO and Ce and Dy co-doped ZnO are shown in Fig. 3. It is clear that the absorption of $\text{Zn}_{0.90}\text{Ce}_{0.05}\text{Dy}_{0.05}\text{O}$ is highest because of the smallest particle size. It can also be seen that the absorbance peak has shifted towards the visible region upon increase in doping concentration. Red shift towards visible region is quite beneficial for improving the photocatalytic properties of ZnO nanoparticles.

The bandgap of un-doped and co-doped zinc oxide nanoparticles was calculated using the formula:

$$\alpha hv = A(hv - E_g)^{1/2}, \quad (4)$$

α here represents the absorption coefficient, A is a constant, hv is the incident photon energy. To calculate the bandgap, $(\alpha hv)^2$ in high absorption range was plotted against hv and linear portion of the graph was extrapolated to $(\alpha hv)^2 = 0$, as shown in Fig. 4. The values of bandgaps were found to be 4.58, 4.55, 4.52, 4.45, 4.4, and 3.6 eV, respectively, for undoped and co-doped ZnO nanoparticles for increasing dopant concentrations. The bandgap decreased from 4.58 to 3.6 eV with increase in co-dopant concentration. Red shift in the absorption edge along with the narrowing of bandgap can be ascribed to the dopants induced creation of oxygen vacancies and creation of additional energy levels in the bandgap of ZnO. This results in increased average atomic distance and decrease in bandgap. Oxygen vacancies as already discussed assist the surface adsorbed oxygen to capture electron which in turn leads to generation of oxide radical. Hence oxygen vacancies lead to better photocatalysis.

Table 2. Calculated lattice parameters (a , c) and crystallite size (d) of un-doped and Ce, Dy co-doped ZnO nanoparticles

Sample	a , Å	c , Å	d , nm
Un-doped	3.196	5.204	47
0.01 M Ce,Dy co-doped	3.240	5.210	39
0.02 M Ce,Dy co-doped	3.243	5.218	36
0.03 M Ce,Dy co-doped	3.247	5.223	34
0.04 M Ce,Dy co-doped ZnO	3.250	5.230	33
0.05 M Ce,Dy co-doped ZnO	3.253	5.241	30

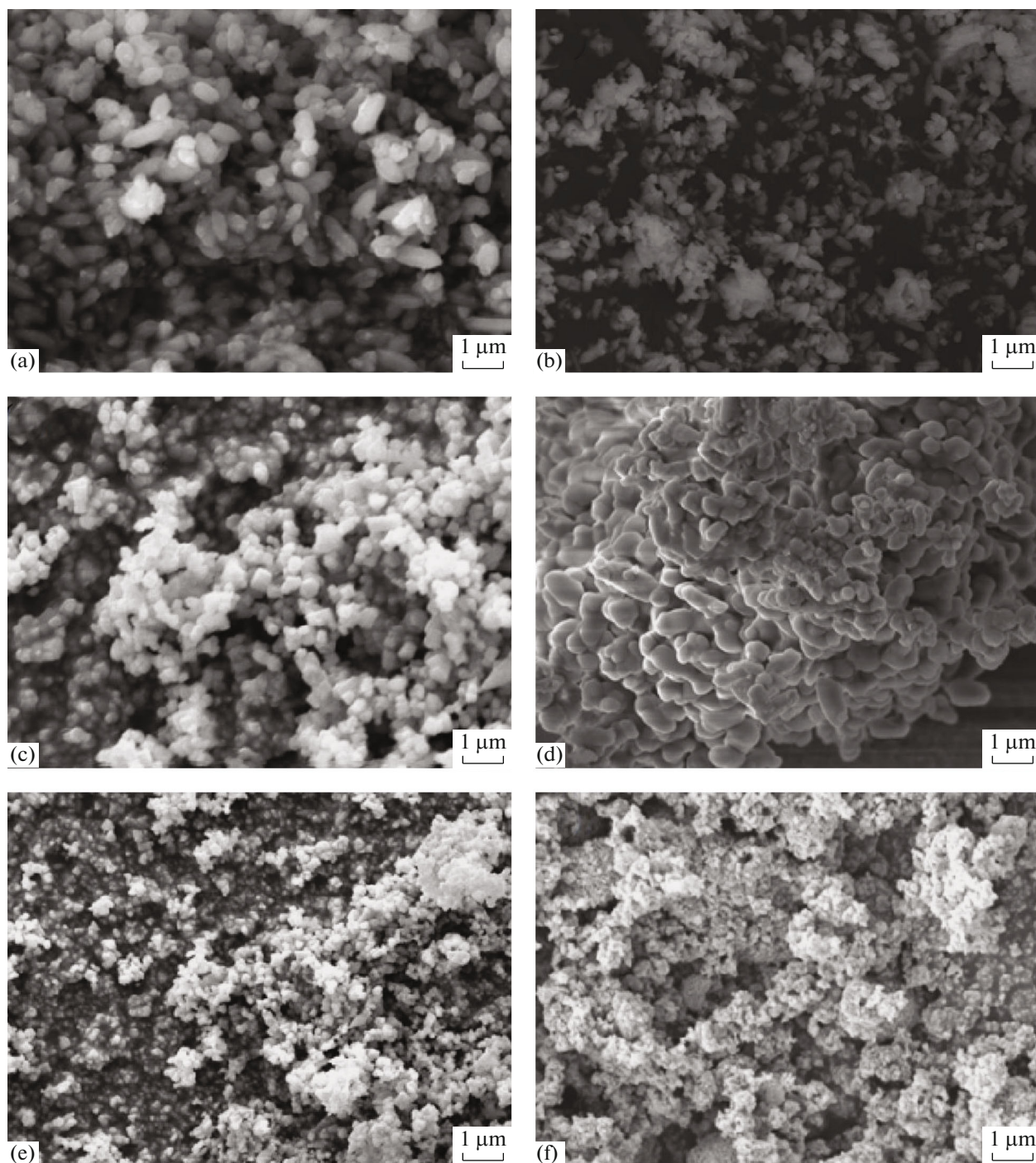


Fig. 2. SEM surface micrographs of un-doped ZnO and Ce,Dy co-doped ZnO nanoparticles; (a) un-doped ZnO, (b) $\text{Zn}_{0.98}\text{Ce}_{0.01}\text{Dy}_{0.01}\text{O}$, (c) $\text{Zn}_{0.96}\text{Ce}_{0.02}\text{Dy}_{0.02}\text{O}$, (d) $\text{Zn}_{0.94}\text{Ce}_{0.03}\text{Dy}_{0.03}\text{O}$, (e) $\text{Zn}_{0.92}\text{Ce}_{0.04}\text{Dy}_{0.04}\text{O}$, and (f) $\text{Zn}_{0.90}\text{Ce}_{0.05}\text{Dy}_{0.05}\text{O}$.

Photoluminescence Studies

The photoluminescence (PL) spectroscopy is a very effective tool for studying various important properties of semiconductor nanomaterials like chemical composition, impurities, bandgap and energy levels. Figure 5a represents the PL spectrum of un-doped and Ce and Dy co-doped ZnO excited at a wavelength

325 nm. Pure or un-doped ZnO shows two emission peaks at 390 and 710 nm, respectively. The peak at the wavelength 390 nm corresponds to UV region of spectrum and can be ascribed to the near band edge emission due to recombination of free and bound excitation pairs. The peak at 710 nm corresponds to the near infra-red region of the spectrum and can possibly

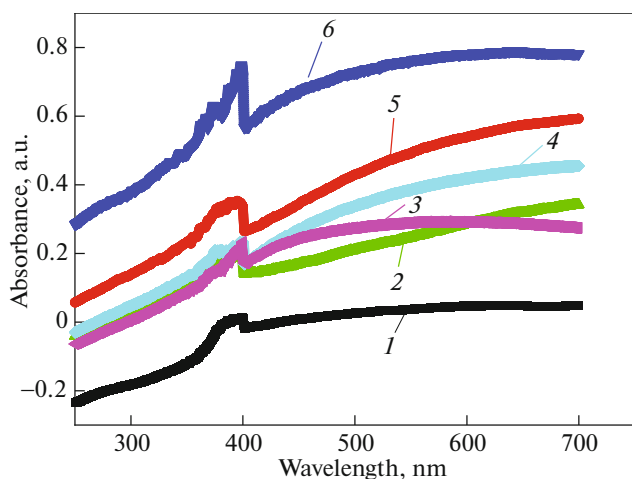


Fig. 3. Optical absorbance spectra of undoped ZnO (1) and Ce, Dy co-doped ZnO nanoparticles (2) $\text{Zn}_{0.98}\text{Ce}_{0.01}\text{Dy}_{0.01}\text{O}$, (3) $\text{Zn}_{0.96}\text{Ce}_{0.02}\text{Dy}_{0.02}\text{O}$, (4) $\text{Zn}_{0.94}\text{Ce}_{0.03}\text{Dy}_{0.03}\text{O}$, (5) $\text{Zn}_{0.92}\text{Ce}_{0.04}\text{Dy}_{0.04}\text{O}$, and (6) $\text{Zn}_{0.90}\text{Ce}_{0.05}\text{Dy}_{0.05}\text{O}$.

appear due to surface plasmon resonance [49]. Two important consequences of Ce and Dy co-doping on the PL spectrum of ZnO are, decreased intensity of the emission peaks in the UV region and their shift towards higher wavelength. Decrease in intensity of emission peaks denotes transfer of energy from host to dopants and confirms perfect substitution of dopant ions into ZnO matrix. Decrease in energy also indicates recombination is prevented as the concentration of dopants increases. As the concentration of dopants increases, the surface bound states act as trap (defect) states as a result relaxation occurs in non radiative manner. The distance between these states and their center-to-center interaction defines the PL intensity. When there is spectral overlap between the wave functions of these states, the energy is transferred in a non-radiative manner, hence there is decrease in intensity [50].

Second important consequence of Ce and Dy co-doping, is that the peak in UV region shifts towards the visible part of the Fraunhofer spectrum as shown in Fig. 5b. This phenomenon can result in efficient utilization of the solar energy and will have important optoelectronic applications. This red shift can possibly be credited to the origination of dopant-induced electronic levels near the conduction band of ZnO. The red shift and consequent bandgap narrowing can also be elucidated on the basis of dopant-induced localized impurity state which merges with the conduction band causing the narrowing of bandgap, as already reported for the Ce doped nitrides [51]. Further, the potential fluctuations caused by the dopants can tailor the valence band and conduction band which causes narrow optical transitions within spin orbital levels that leads to narrowing of the bandgap [52]. Also, the Pauli

electronegativities of Dy^{3+} (1.22) and Ce^{3+} (1.12) are less than that of Zn^{2+} (1.65). Acceptor bound excitation pair is generated due to coulombic interaction between electron-hole pairs bound by the isoelectronic levels formed by Ce and Dy. So there is charge transfer between conduction band of ZnO and different states of Ce and Dy. This can also lead to bandgap narrowing and red shift in Ce and Dy co-doped ZnO nanoparticles [53].

Photocatalytic Studies

Photocatalytic activity of pure and Ce and Dy co-doped ZnO nanoparticles were measured through photolytic degradation of Rhodamine B dye under UV light irradiation. The degradation of Rhodamine B dye with photocatalysts, ZnO and Ce and Dy co-doped ZnO nanoparticles is depicted in Fig. 6 at different reaction times (0–60 min). As the doping concentration increases, the absorbance of dye gets decreased with reaction time. The degradation is fastest and most efficient with $\text{Zn}_{0.90}\text{Ce}_{0.05}\text{Dy}_{0.05}\text{O}$ photocatalyst.

Figure 7a reveals the photocatalytic performance of the undoped and Ce and Dy co-doped ZnO nanoparticles in degradation of the same dye. The photocatalytic performance is shown as the plot between C_t/C_0 and irradiation time (t), where C_0 represents the initial dye concentration and C_t denotes the residual dye concentration at time t . The photocatalytic degradation of Rhodamine B dye roughly follows the pseudo-first order kinetics with lower concentrations of dye [54]:

$$\ln[C_t/C_0] = Kt. \quad (5)$$

In the above equation value K is the kinetic parameter for different photocatalysts. The value of apparent constant K can be estimated by linear fitting the slope of graph of $\ln(C_t/C_0)$ vs. irradiation time t as depicted in Fig. 7b. The values of K were estimated to be 0.0247, 0.039, 0.0411, 0.0321, 0.0351, and 0.0428 s^{-1} for undoped ZnO and $\text{Zn}_{0.98}\text{Ce}_{0.01}\text{Dy}_{0.01}\text{O}$, $\text{Zn}_{0.96}\text{Ce}_{0.02}\text{Dy}_{0.02}\text{O}$, $\text{Zn}_{0.94}\text{Ce}_{0.03}\text{Dy}_{0.03}\text{O}$, $\text{Zn}_{0.92}\text{Ce}_{0.04}\text{Dy}_{0.04}\text{O}$, $\text{Zn}_{0.90}\text{Ce}_{0.05}\text{Dy}_{0.05}\text{O}$, respectively. The value of apparent constant K is highest for $\text{Zn}_{0.90}\text{Ce}_{0.05}\text{Dy}_{0.05}\text{O}$. The efficiency of the photocatalysts was further estimated by calculating the degradation percentage using the formula given below:

$$D, \% = (1 - C_t/C_0) \times 100, \quad (6)$$

where D is the degradation percentage, C_0 and C_t are the initial and residual dye concentrations, respectively. The degradation percentage was highest (98%) with $\text{Zn}_{0.90}\text{Ce}_{0.05}\text{Dy}_{0.05}\text{O}$ photocatalyst, as shown in Fig. 7c. The decrease in particle with increased dopant

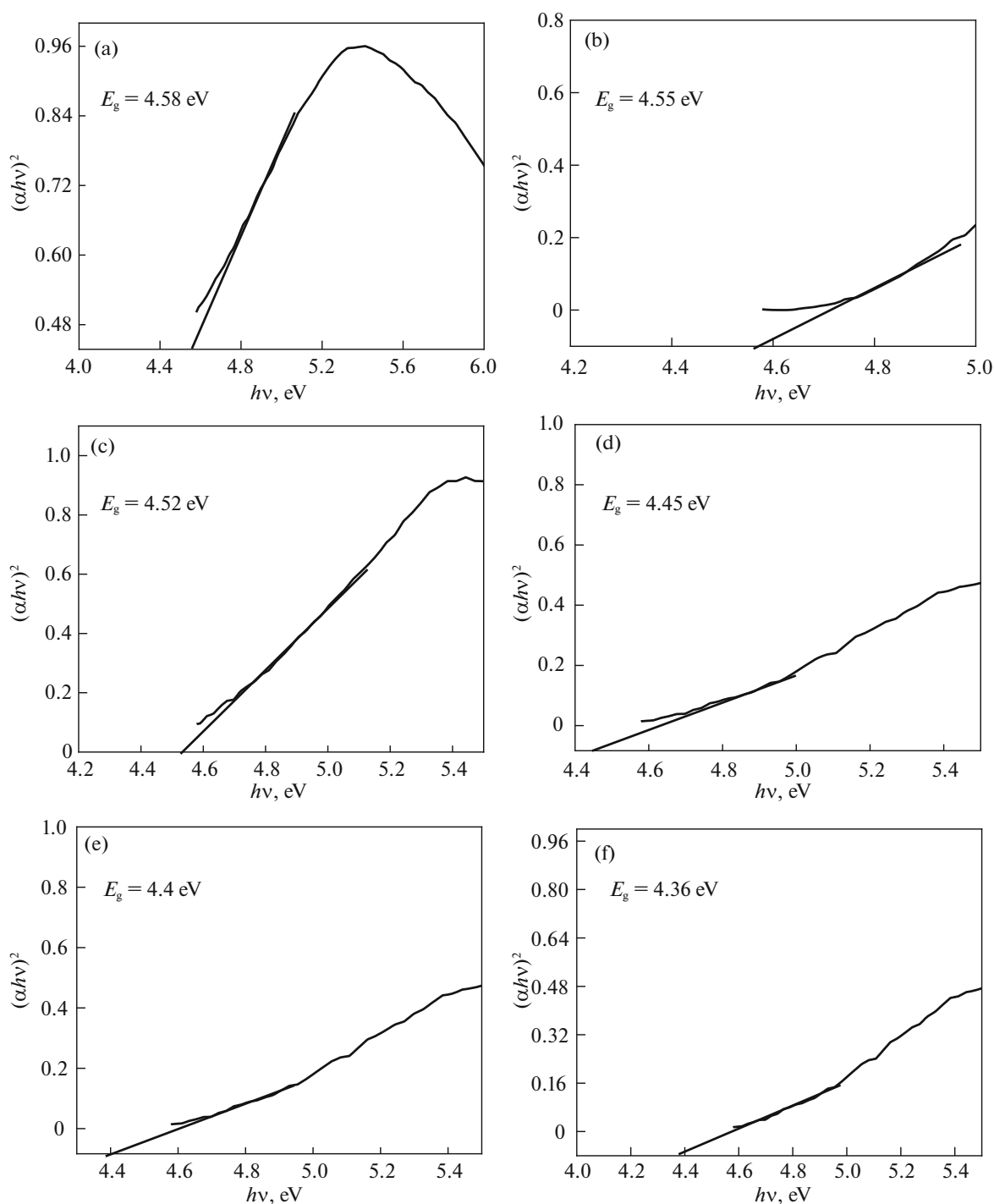


Fig. 4. The $(\alpha hv)^2$ vs. $h\nu$ diagram for the optical energy band gap determination of undoped ZnO and Ce,Dy co-doped ZnO nanoparticles; (a) un-doped ZnO, (b) $Zn_{0.98}Ce_{0.01}Dy_{0.01}O$, (c) $Zn_{0.96}Ce_{0.02}Dy_{0.02}O$, (d) $Zn_{0.94}Ce_{0.03}Dy_{0.03}O$, (e) $Zn_{0.92}Ce_{0.04}Dy_{0.04}O$, and (f) $Zn_{0.90}Ce_{0.05}Dy_{0.05}O$.

concentration leads to an increased surface area and eventually enhanced photocatalytic activity.

Enhancement of photocatalytic activity with Ce and Dy co-doping can be understood by looking at the degradation mechanism as follows. Initially the semi-

conductor nano-photocatalyst under consideration is excited with photons having energy $h\nu >$ bandgap. Excitation generates the electron-hole pairs on the surface of semiconductor. The photo-generated electrons are trapped by the O_2 adsorbed on the surface of

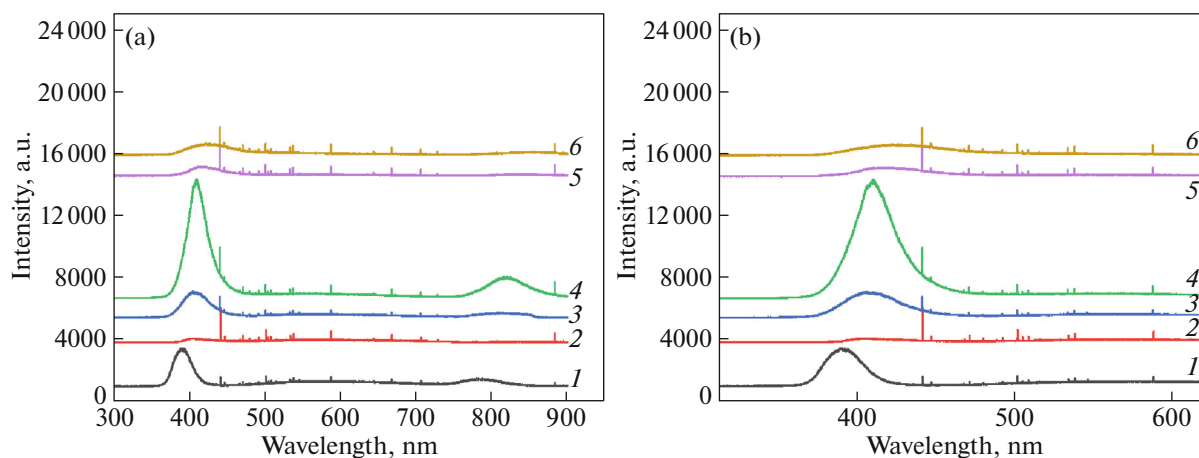
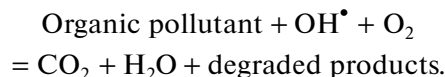
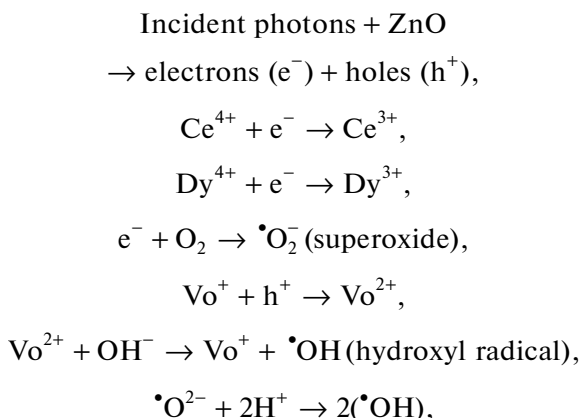


Fig. 5. (a) Room temperature PL spectrum of undoped (1) and Ce,Dy co-doped ZnO nanoparticles (2— $\text{Zn}_{0.98}\text{Ce}_{0.01}\text{Dy}_{0.01}\text{O}$, 3— $\text{Zn}_{0.96}\text{Ce}_{0.02}\text{Dy}_{0.02}\text{O}$, 4— $\text{Zn}_{0.94}\text{Ce}_{0.03}\text{Dy}_{0.03}\text{O}$, 5— $\text{Zn}_{0.92}\text{Ce}_{0.04}\text{Dy}_{0.04}\text{O}$, and 6— $\text{Zn}_{0.90}\text{Ce}_{0.05}\text{Dy}_{0.05}\text{O}$); (b) expanded UV region of the spectrum showing red shift with increase in concentration of dopants.

nanoparticles, this is the rate determining step in photocatalysis. The $4f$ configuration of co-dopants Ce and Dy plays the most important role in generation, charge transfer and inhibition of electron–hole recombination. Ce^{4+} and Dy^{4+} act as scavengers for the electrons from conduction band. In addition, Ce^{4+} and Dy^{4+} also act as stronger Lewis acids as compared to O_2 and are better at trapping electrons adsorbed by O_2 . Hence the co-dopants trap electrons, which by oxidative process get transferred to surface adsorbed oxygen and produce superoxide radical ion ($\cdot\text{O}_2^-$). Also, the photoinduced electrons and holes can easily recombine and dissipate the energy as heat in absence of a defect state. Defect states prevent this from happening. In the current work, electron–hole separation is enhanced by the presence of single oxygen vacancies (Vo^+) in the bandgap of ZnO. Oxygen vacancy acts as an electron donor and forms charged oxygen vacancy which acts as a trap for holes, thereby preventing the recombination. Charged oxygen vacancy upon reaction with (OH^-) forms $(\text{OH}\cdot)$, which can also be formed reaction of superoxide anion with hole. This can be written as,



Oxygen vacancies in addition to trapping the holes also help in adsorbing oxygen, hence presence of oxygen vacancies greatly enhances photocatalysis [55]. The efficiency of photocatalysts thus depends on a number of factors, such as number of charge carriers at the surface of photocatalyst and electron–hole recombination rate, which in turn depends on the bandgap. In the current work, photocatalytic efficiencies of Ce and Dy co-doped ZnO nanoparticle based photocatalysts are enhanced many fold as compared to un-doped ZnO photocatalysts, with $\text{Zn}_{0.90}\text{Ce}_{0.05}\text{Dy}_{0.05}\text{O}$ exhibiting the best results. The reason for much improved photocatalytic ability of Ce and Dy co-doped ZnO nanoparticles can be ascribed to loading of the dopant ions on the surface of host particles and availability of oxygen vacancies due to Ce, Dy co-doping as a result of which, there is accelerated transport of charge carriers (electrons) to the adsorbed oxygen molecules. Further, more charge carriers are available on the surface due to decreased size and increased surface area as is clear from the SEM analysis (Fig. 2).

The photoluminescence study of Ce and Dy Co-doped ZnO also revealed the shift of absorption edge towards the visible portion of solar spectrum and consequent bandgap narrowing which eventually can lead to better utilization of solar energy and hence more efficient photocatalysis (Figs. 5a, 5b). Further, photoluminescence study reveals incorporation of additional levels in the bandgap of ZnO due to Ce and Dy co-doping which delays the recombination of charge carriers, which also contributes to enhanced degrada-

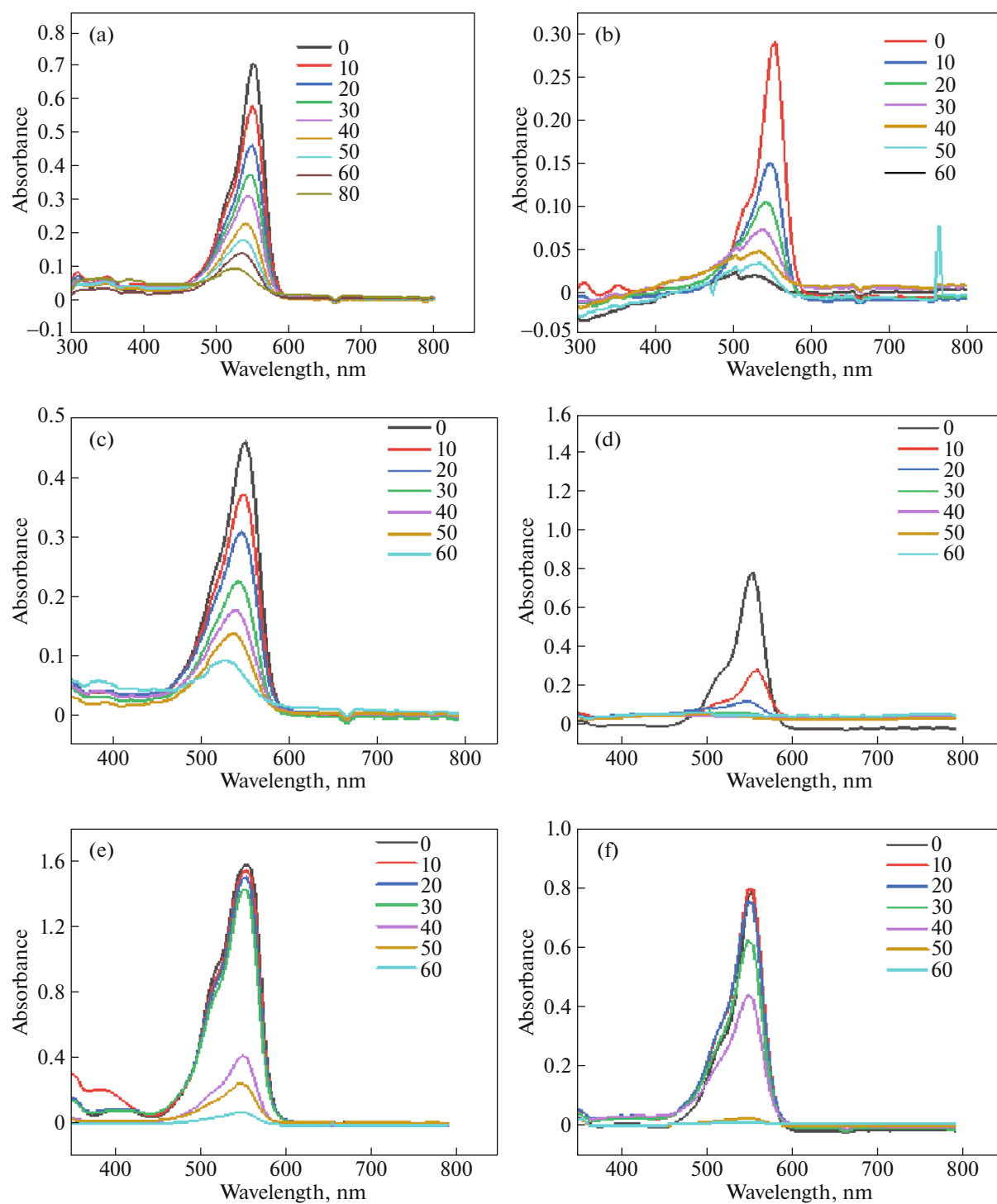


Fig. 6. UV–Vis spectral changes of Rhodamine B dye solution during photocatalytic degradation with un-doped and Ce,Dy co-doped ZnO nanoparticles under UV irradiation at different time intervals (min); (a) un-doped ZnO, (b) $Zn_{0.98}Ce_{0.01}Dy_{0.01}O$, (c) $Zn_{0.96}Ce_{0.02}Dy_{0.02}O$, (d) $Zn_{0.94}Ce_{0.03}Dy_{0.03}O$, (e) $Zn_{0.92}Ce_{0.04}Dy_{0.04}O$, and (f) $Zn_{0.90}Ce_{0.05}Dy_{0.05}O$.

tion of rhodamine B dye. The red shift of the absorption band and the narrowing of bandgap is also confirmed by the UV–Vis analysis of un-doped and Ce and Dy co-doped ZnO nanoparticles.

CONCLUSION

Facile and cost effective co-precipitation technique was successfully utilized to obtain pure and Ce and Dy co-doped ZnO nanoparticles. XRD analysis

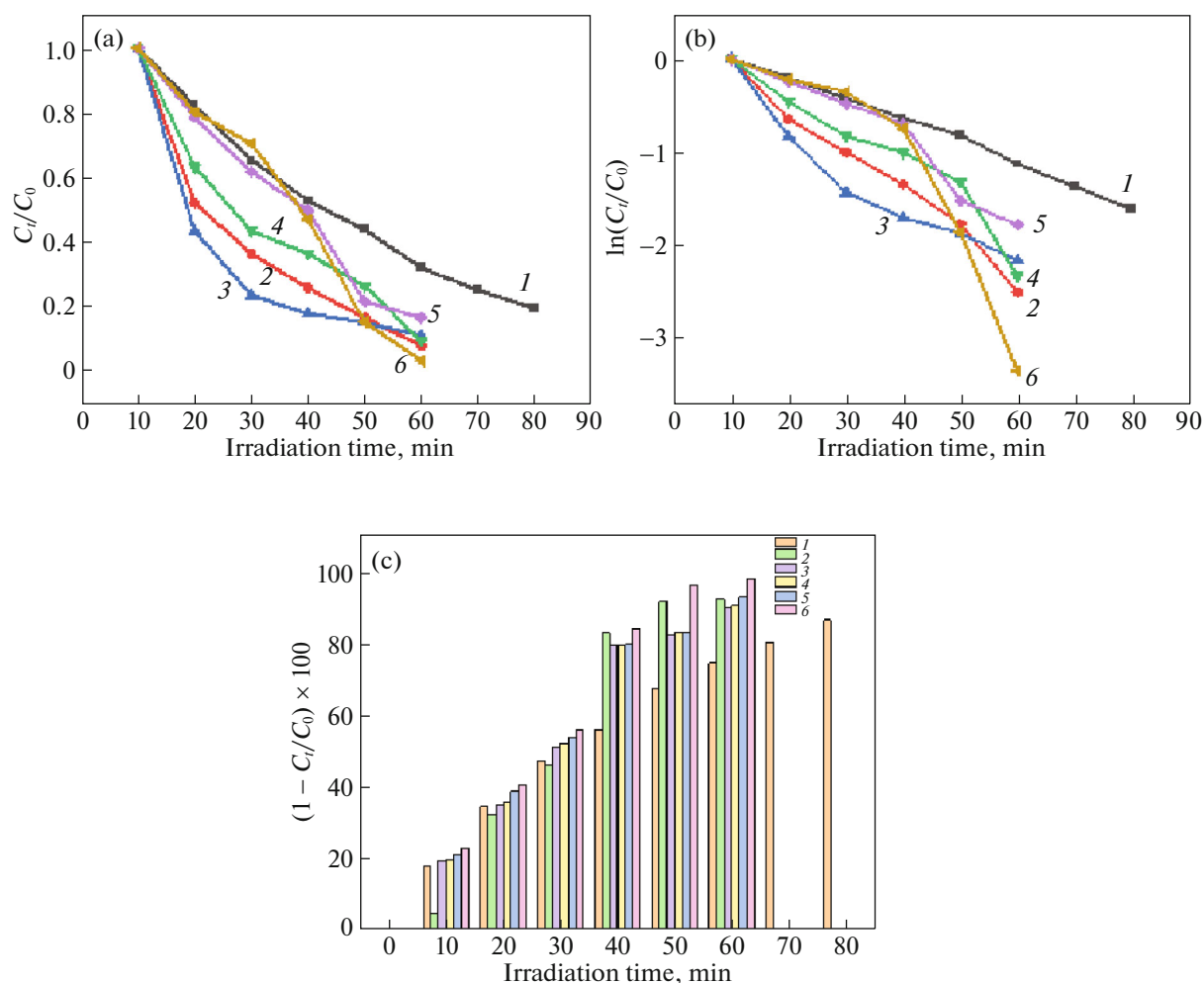


Fig. 7. (a) Photocatalytic degradation of Rhodamine B dye solution un-doped (1) and Ce,Dy co-doped ZnO nanoparticles (2— $\text{Zn}_{0.98}\text{Ce}_{0.01}\text{Dy}_{0.01}\text{O}$, 3— $\text{Zn}_{0.96}\text{Ce}_{0.02}\text{Dy}_{0.02}\text{O}$, 4— $\text{Zn}_{0.94}\text{Ce}_{0.03}\text{Dy}_{0.03}\text{O}$, 5— $\text{Zn}_{0.92}\text{Ce}_{0.04}\text{Dy}_{0.04}\text{O}$, and 6— $\text{Zn}_{0.90}\text{Ce}_{0.05}\text{Dy}_{0.05}\text{O}$); (b, c) reaction kinetics of photocatalytic degradation with un-doped ZnO nanoparticles and Ce,Dy co-doped ZnO nanoparticles under UV irradiation at different time intervals.

confirmed successful formation of pure and co-doped ZnO nanoparticles with slight distortion of lattice in co-doped samples due to mismatch of ionic radii of host and dopant ions. The average particle size was calculated to be 35 nm. Morphological studies revealed formation of flower shaped nanoparticles with increase in concentration of Ce and Dy co-dopants. The photoluminescence studies revealed narrowing of bandgap and that the emission could be tuned because of Ce and Dy co-doping. Further, red shift towards visible region was observed as doping concentration was increased, making the nanoparticles efficient candidates for optoelectronic and photocatalytic applications. Photocatalytic studies showed that Ce and Dy co-doped ZnO nanoparticles had much improved photocatalytic performance than un-doped ZnO. The recombination rate of photogenerated charge carriers was suppressed in Ce, Dy co-doped samples due to incorporation of trap levels,

increased surface oxygen vacancies and charge transfer. As a consequence, the photocatalytic activity of co-doped nanoparticles was found to be exceedingly enhanced in comparison to un-doped ZnO nanoparticles for the degradation of Rhodamine B dye with $\text{Zn}_{0.90}\text{Ce}_{0.05}\text{Dy}_{0.05}\text{O}$ exhibiting the highest activity.

REFERENCES

1. P. Thiagarajan, M. Kottaisamy, K. Sethupathi, and M. S. R. Rao, *J. Displays* **30**, 202 (2009).
2. C. Zhang and J. Lin, *Chem. Soc. Rev.* **41**, 7938 (2012).
3. M. Shang, G. Li, D. Yang, X. Kang, C. Peng, Z. Cheng, and J. Lin, *Dalton Trans.* **40**, 9379 (2011).
4. P. V. Korake, R. S. Dhabbe, A. N. Kadam, Y. B. Gaikwad, and K. M. Garadkar, *J. Photochem. Photobiol. B* **130**, 11 (2014).

5. Ü. Özgür, Y. I. Alivov, C. Liu, A. Teke, M. A. Reshchikov, S. Doğan, V. Avrutin, S. J. Cho, and H. Morkoç, *J. Appl. Phys.* **98**, 041301 (2005).
6. U. O. H. Morkoc, *Zinc Oxide: Fundamentals, Materials, and Device Technology* (Wiley, Hoboken, 2009).
7. S. Baskoutas and G. Bester, *J. Phys. Chem. C* **114**, 9301 (2010).
8. S. C. Erwin, L. Zu, M. I. Haftel, A. L. Efros, T. A. Kennedy, and D. J. Norris, *Nature (London, U. K.)* **436**, 91 (2005).
9. D. J. Norris, A. L. Efros, and S. C. Erwin, *Science (Washington, DC, U. S.)* **319**, 1776 (2008).
10. K. Yim, J. Lee, D. Lee, M. Lee, E. Cho, H. S. Lee, H.-H. Nahm, and S. Han, *Sci. Rep.* **7**, 40907 (2017).
11. T. Makino, Y. Segawa, S. Yoshida, A. Tsukazaki, A. Ohtomo, and M. Kawasaki, *Appl. Phys. Lett.* **85**, 759 (2008).
12. S. Singh, N. Rama, and M. S. R. Rao, *Appl. Phys. Lett.* **88**, 222111 (2006).
13. A. Azarov, A. Galeckas, A. Hallén, A. Kuznetsov, E. Monakhov, and B. G. Svensson, *J. Appl. Phys.* **118**, 125703 (2015).
14. A. Kunz, P. Peralta-Zamora, S. G. de Moraes, and N. Duran, *Quim. Nova* **25**, 78 (2002).
15. P. V. Korake, A. N. Kadam, and K. M. Garadkar, *J. Rare Earths* **32**, 306 (2014).
16. N. Shaari, S. H. Tan, and A. R. Mohamed, *J. Rare Earths* **30**, 651 (2012).
17. X. J. Yu, L. L. Xiong, G. P. Ma, Y. Liang, and K. R. Liu, *J. Rare Earths* **32**, 849 (2014).
18. C. Wang and L. Cao, *J. Rare Earths* **29**, 727 (2011).
19. J. Wu, G. L. Zhang, J. Liu, H. B. Gao, C. X. Song, H. R. Du, Z. Li, Z. P. Gong, and Y. G. Lu, *J. Rare Earths* **32**, 727 (2014).
20. A. L. Linsebigler, G. Q. Lu, and J. T. Yates, Jr., *Chem. Rev.* **95**, 735 (1995).
21. M. Romero, J. Blanco, B. Sanchez, A. Vidal, S. Malato, A. I. Cardona, et al., *Sol. Energy* **66**, 169 (1999).
22. M. Ahmad, E. Ahmed, Z. L. Hong, J. F. Xu, N. R. Khalid, A. Elhissi, and W. Ahmed, *J. Alloys Compd.* **577**, 717 (2013).
23. M. Ahmad, E. Ahmed, Z. L. Hong, Z. Iqbal, N. R. Khalid, T. Abbas, I. Ahmad, A. Elhissi, and W. Ahmed, *Ceram. Int.* **39**, 8693 (2013).
24. M. Ahmad, E. Ahmed, Z. L. Hong, X. L. Jiao, T. Abbas, and N. R. Khalid, *Appl. Surf. Sci.* **285**, 702 (2013).
25. H. S. Cai, G. G. Liu, W. Y. Lu, X. X. Li, L. Yu, and D. G. Li, *J. Rare Earths* **26**, 71 (2008).
26. S. Kumar and P. D. Sahare, *J. Rare Earths* **30**, 761 (2012).
27. D. K. Sharma, K. K. Sharma, V. Kumar, and A. Sharma, *J. Mater. Sci.: Mater. Electron.* **27**, 10330 (2016).
28. Q. Shi, C. Wang, S. Li, Q. Wang, B. Zhang, W. Wang, J. Zhang, and H. Zhu, *Nanoscale Res. Lett.* **9**, 480 (2014).
29. M. Ahmad, E. Ahmed, F. Zafar, N. R. Khalid, N. A. Niaz, A. Hafeez, M. Ikram, M. A. Khan, and Z. Hong, *J. Rare Earths* **33**, 255 (2015).
30. N. C. S. Selvam, J. J. Vijaya, and L. J. Kennedy, *J. Nanosci. Nanotechnol.* **13**, 1 (2013).
31. S. Rajendran, M. M. Khan, F. Gracia, J. Qin, V. K. Gupta, and S. Arumainathan, *Sci. Rep.* **6**, 31641 (2016).
32. H. X. Shi, T. Y. Zhang, and H. L. Wang, *J. Rare Earths* **29**, 746 (2011).
33. R. Zeng, J. G. Wang, J. Y. Cui, L. Hu, and K. G. Mu, *J. Rare Earths* **28**, 353 (2010).
34. C. M. Fan, P. Xue, and Y. P. Sun, *J. Rare Earths* **24**, 309 (2006).
35. L. Bian, M. X. Song, T. L. Zhou, X. Y. Zhou, and Q. Q. Dai, *J. Rare Earths* **27**, 461 (2009).
36. M. Zalaj, *J. Rare Earths* **32**, 487 (2014).
37. R. K. Kalaiezhily, V. Asvini, G. Saravanan, and K. Ravichandran, *Dalton Trans.* **48**, 12228 (2019).
38. J. Iqbal, X. Liu, H. Zhu, Z. B. Wua, Y. Zhang, D. Yu, and R. Yu, *Acta Mater.* **57**, 4790 (2009).
39. P. Pascariu, M. Homocianu, C. Cojocaru, P. Samoila, A. Airinei, and M. Suche, *Appl. Surf. Sci.* **476**, 16 (2019).
40. M. Romero, J. Blanco, B. Sanchez, A. Vidal, S. Malato, A. I. Cardona, et al., *Sol. Energy* **66**, 169 (1999).
41. A. Rahman and R. Jayaganthan, *Trans. Indian Inst. Met.* **70**, 1063 (2016).
42. C. A. Arguello, D. L. Rousseau, and S. P. S. Porto, *Phys. Rev.* **181**, 351 (1969).
43. R. Bomila, S. Suresh, and S. Srinivasan, *J. Mater. Sci: Mater. Electron.* **30**, 582 (2019).
44. X. Z. Li, F. B. Li, C. L. Yang, and W. K. Ge, *J. Photochem. Photobiol. A* **141**, 209 (2009).
45. L. Q. Jing, X. J. Sun, W. M. Cai, Z. L. Xu, Y. G. Du, and H. G. Fu, *J. Phys. Chem. Solid* **64**, 615 (2003).
46. H. Yamashita, Y. Ichihashi, S. G. Zhang, Y. Matsumurab, Y. Soumab, T. Tatsumic, et al., *Appl. Surf. Sci.* **121**, 305311 (1997).
47. R. Bomila, S. Srinivasan, A. Venkatesan, B. Bharath, and K. Perinbam, *Mater. Res. Innov.* **22**, 379 (2017).
48. X. Liu, D. G. Sroppa, M. Heggan, Y. Ermolenko, A. Offenhausser, and Y. Mourzina, *J. Phys. Chem. C* **119**, 10336 (2015).
49. J. H. Zeng, Y. L. Yu, Y. F. Wang, and T. Lou, *J. Acta. Mater.* **57**, 1813 (2009).
50. A. George, S. K. Sharma, S. Chawla, M. M. Malik, and M. S. Qureshi, *J. Alloys Compd.* **509**, 5942 (2011).
51. A. Majid and A. Ali, *J. Phys. D: Appl. Phys.* **42**, 45412 (2009).
52. K. F. Berggren and B. E. Sernelius, *Phys. Rev.* **24**, 1971 (1981).
53. S. Bhatia and N. Verma, *Mater. Res. Bull.* **95**, 468 (2017).
54. S. Wang, L. Bai, and X. Ao, *RSC Adv.* **8**, 36745 (2018).
55. C. J. Chang, C. Y. Lin, and M. H. Hsu, *J. Taiwan. Inst. Chem. Eng.*, **45**, 1954 (2014).